AFRL-VS-TR-1999-1512

Space Systems Environmental Interaction Studies

M. Alan Morgan
Alan C. Huber
David J. Sperry

Alan N. Donkin, Jr.
Scott J. Moran
M. Paul Gough

John A. Pantazis

AMPTEK, Inc.
6 DeAngelo Drive
Bedford, MA 01730

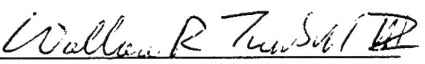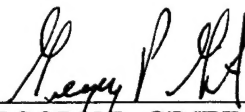30 August 1998

Scientific Report No. 2

20020603 066

AIR FORCE RESEARCH LABORATORY
Space Vehicles Directorate
29 Randolph Rd
AIR FORCE MATERIEL COMMAND
Hanscom AFB, MA 01731-3010

" This technical report has been reviewed and is approved for publication."

WALLACE R. TURNBULL, Capt, USAF
Contract Manager

GREGORY P. GINET, Chief
Space Weather Center of Excellence

REPORT DOCUMENTATION PAGE

Public reporting burden for this collection of information is estimated to average 1 hour per response, including the time for reviewing instructions, searching existing data sources, gathering and maintaining the data needed, and completing and reviewing the collection of information. Send comments regarding this burden estimate or any other aspect of this collection of information, including suggestions for reducing this burden, to Washington Headquarters Services, Directorate for Information Operations and Reports, 1215 Jefferson Davis Highway, Suite 1204, Arlington, VA 22202-4302, and to the Office of Management and Budget, Paperwork Reduction Project (0704-0188), Washington, DC 20503.

1. AGENCY USE ONLY (Leave blank)	2. REPORT DATE	3. REPORT TYPE AND DATES COVERED
	30 August 1998	Scientific No. 2

4. TITLE AND SUBTITLE

Space Systems Environmental Interaction Studies

5. FUNDING NUMBERS

PE: 63410F

PR 2822 GCDD

Contract F19628-96-C-0144

6. AUTHOR(S)

M. Alvin Morgan   Alan N. Donkin Jr.   John A. Pantazis
Alan C. Huber   Scott J. Moran
David J. Sperry   M. Paul Gough

7. PERFORMING ORGANIZATION NAME(S) AND ADDRESS(ES)

AMPTEK, Inc.
6 DeAngelo Drive
Bedford, MA 01730-2204

8. PERFORMING ORGANIZATION REPORT NUMBER

9. SPONSORING/MONITORING AGENCY NAME(S) AND ADDRESS(ES)

Air Force Research Laboratory
29 Randolph Road
Hanscom AFB, MA 01731-3010

Contract Manager: Lt. Perter Berkley /VSBS

10. SPONSORING/MONITORING AGENCY REPORT NUMBER

AFRL-VS-TR-99-1512

11. SUPPLEMENTARY NOTES

12a. DISTRIBUTION/AVAILABILITY STATEMENT

Approved for public release; Distribution unlimited

12b. DISTRIBUTION CODE

13. ABSTRACT (Maximum 200 words)

Development efforts for the DIDM-2 instrument, which occurred under Task 1 of this contract, are reported. Details on various hardware elements are presented. On-going data analysis efforts contracted under Task 2, regarding the SPREE and OEDIPUS-C data sets is reported. A look at the off-shoot software analysis tool developed for the LaTUR data set is presented. Under Task 3 (the Langmuir TURbulence [LaTUR] rocket investigation program), final details are given of the hardware provided to the now-concluded efffort.

14. SUBJECT TERMS

Digital Ion Drift Meter, DIDM, CHallenging Mini-satellite Program, CHAMP
OEDIPUS-C Data Analysis software, Energetic Particle Instrument, EPI
Langmuir TURbulence investigation, LaTUR

15. NUMBER OF PAGES

16. PRICE CODE

17. SECURITY CLASSIFICATION OF REPORT	18. SECURITY CLASSIFICATION OF THIS PAGE	19. SECURITY CLASSIFICATION OF ABSTRACT	20. LIMITATION OF ABSTRACT
Unclassified	Unclassified	Unclassified	SAR

Table of Contents

List of Figures

1. INTRODUCTION

This contract's objective is to further the understanding of near-earth environmental dynamics, by conducting both *In Situ* experimental studies, as well as, analytical and empirical studies of returned instrument data. The work is to be accomplished through three programs, subsequently identified as Task #'s 1, 2 and 3. A brief review of the scope of each program and a summary of the work performed during the report period follows. The material is presented in serial order, with Task #1 issues appearing first in Section 2.

2. TASK #1—DIDM EFFORTS

2.1 Program Definition

The objectives of this task are two-fold. They are: (1) develop the means to reliably measure ion densities in the range of 10^1 cm^{-3} to 10^7 cm^{-3}, by using digital rather than analog techniques, and thereby extend the existing dynamic range for such measurements by at least three orders of magnitude. (2) determine the incident angle of ions into the instrument within 3° in two dimensions, to allow accurate determination of ion drift velocities.

The work performed during the report period falls within Phase 3 of this task, under which a Digital Ion Drift Meter (DIDM) instrument is to be fabricated, tested and calibrated. The instrument is built for AFRL and is to be delivered to the German research organization GeoForschungsZentrum (GFZ), for inclusion in their earth studies research satellite CHAllenging Minisatellite Payload (CHAMP) instrument suite. DIDM will be integral to the global earth magnetic and electric field mapping aspect of the CHAMP mission, and it is expected to make a contribution in furthering the understanding of solar-terrestrial physics.

2.2 Summary of Activities

Phase 3 work proceeded in earnest during the report period. The impetus was the scheduled instrument delivery date of 15 July, which GFZ repeatedly emphasized throughout, would not change. All outstanding issues relating to hardware design were resolved by the first quarter and two sets of both the DIDM instrument housing and the Planar Langmuir Probe (PLP) were fabricated. The electronics design was finalized shortly thereafter as well, and printed circuit boards were manufactured for both instruments. Subsequently, these were populated with electrical components and the full instrument electronics assemblies were built-up. Of the two units, one was identified as the engineering unit and used principally for hardware debugging and software development work. It was also used for instrument qualification and initial characterization testing. The other unit was earmarked for delivery as the flight unit and therefore treated accordingly. Additional details on DIDM hardware is provided in section 2.3.

Some time was spent verifying the proper functionality of the completed engineering unit, before the flight unit was actually put together and checked out. The two units were then subjected to the required environment test exercises, almost immediately. Due to time constraints, and with the consent of AFRL and GFZ, both the flight and engineering units were used to qualify the instrument design in the environment tests. For instance, while the flight unit was undergoing a magnetic survey at the NASA–Goddard space flight test facility in Maryland, the engineering unit was being subjected to the required electromagnetic interference (EMI) and electromagnetic compatibility (EMC) tests, in Nashua, New Hampshire. The engineering unit was also used in the thermal vacuum and qualification vibration tests, while the flight unit was simultaneously engaged in initial instrument characterization test exercises.

Special diagnostic software was written to monitor these tests. The structure of the defined instrument output is such that flight software would not be the most useful diagnostic means for the job anyway. A typical GSE display as seen with that version of the software is shown in Figure 1. It indicates the status of the essential instrument parameters only, and as will be seen shortly, is quite a bit different from the comprehensive GSE display developed for the flight software.

```
Sync:DIDM MF:0048 Test_Status:88 DPU_Status:02        Pulser:ON
ADC 0 :022E ADC 1 :0000 ADC 2 :01FD ADC 3 :07FF       Image:DM1
              Electrometer= 4997.6µA                  HV:OFF
DM1:14370 GATE1:14371 RPA1: 14370                     LVMON= 2.486V
PEAK1:10171 at  57,11 - actual=10171, Total=14370     HVMON= 0.000V
Quad1_0:     2 Quad1_1:14368 Quad1_2:     0 Quad1_3:  0 TEMP= 29.6C

DM2:14370 GATE2:14371 RPA2: 14370
PEAK2:10692 at  61, 9 - actual=?????, Total=?????
Quad2_0:     2 Quad2_1:14368 Quad2_2:     0 Quad2_3:  0

44 49 44 4D 48 00 88 2E 02 00 00 FD 01 FF 07 02 22 38 23 38 22 38 22 38 23 38 22
 38 39 CB 3D C9 BB 27 C4 29 02 00 20 38 00 00 00 00 02 00 20 38 00 00 00 00 02
00 00 00 00 00 00 00 00 00 00 00                    █ 7769 - 16390
                                                    ░ 3683 - 7768
                                                    ▒ 1745 - 3682
                                                    ┄ 827 - 1744
                                                    ▐ 392 - 826
                                                    █ 185 - 391
                                                    ▓ 88 - 184
                                                    ░ 41 - 87
                                                      19 - 40
                                                       9 - 18
                                                       4 - 8
                   ▐▌                                  2 - 3
                                                       1 - 1

F1:Pulser ON F2:Pulser OFF F3:DM1 image F4:DM2 image Alt-H:HV ON SPACE:HV OFF
ALT-Q to quit  LEN= 4148                            COM2:19200,N,8,1
```
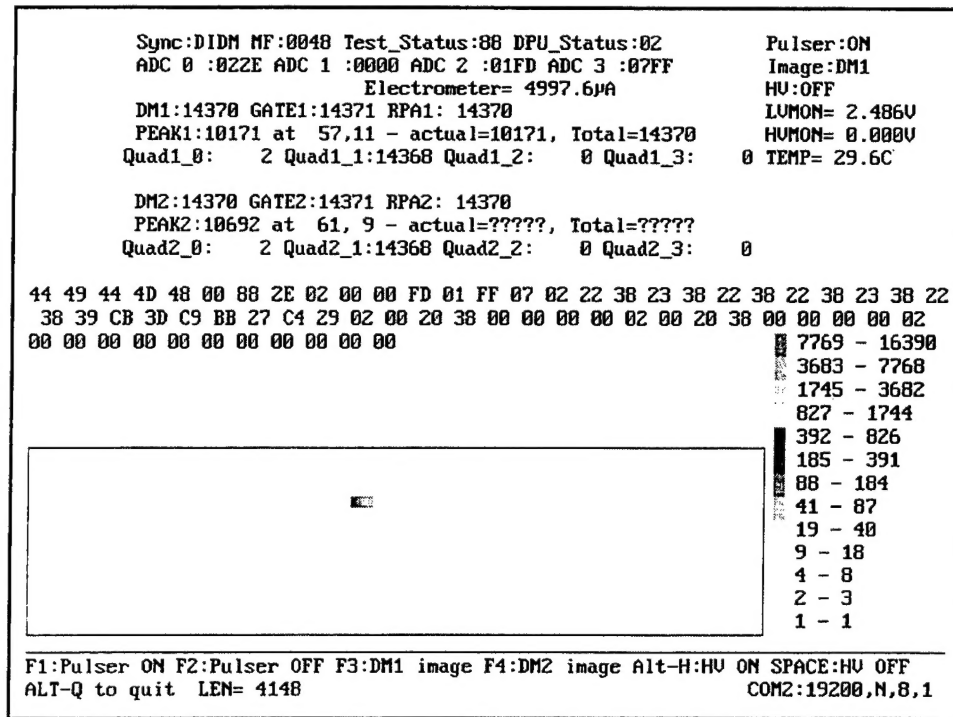
FIGURE 1: DIAGNOSTIC SOFTWARE GSE DISPLAY

Work on the flight software progressed steadily in the latter half of the report period. The code is written in modular fashion, with specific features incorporated as needed or as the functionality of the particular algorithm is defined and developed. It was important to have a version of the flight software up and running for the initial instrument characterization tests, as contrary to previous instrument development efforts, the DIDM GSE display software that was used during the instrument characterization and calibration exercises, was developed by another vendor. It was therefore necessary for proper instrument-GSE interfacing that the nominal output from the instrument be present. Thus the final structure of the instrument output had to be in place, with telemetry items appearing in the correct location, even if most locations were zero filled. For the instrument characterization tests, it was only necessary to have the instrument housekeeping and drift meter image data features fully functional, and this was done.

A key feature of the DIDM-2 development effort was the ability to remotely upload new versions of the operating software to the instrument. This made it possible to put the latest version of the code into the instrument, at any convenient time. It could be done while the instrument was still in the test chamber for example, and greatly aided the characterization and calibration process, in terms of the time made available to exercise the instrument. Unlike the manner in which the matter was handled in the past, it is no longer necessary to lose at least a day of test time in having to take the instrument out of the test chamber, opening it up to replace the PROM in which the operational software resides, reinstalling the instrument in the test chamber and waiting at least twenty four hour period for the sensors to properly outgas, before testing can resume. Rather, the latest software can be transferred from the developer's PC at Amptek, via the File Transfer Protocol (FTP) on the internet,

directly to the remotely located GSE laptop computer which controls the instrument. In a timespan of seconds, the new code can then be loaded into the instrument and immediately thereafter calibration activities can resume. Considerably more instrument runtime is now afforded with this ability, to evaluate new software and to conduct a more exhaustive test campaign.

First the engineering unit, and then the flight unit, were handed over to AFRL for initial characterization and calibration testing. The rush to complete these exercises abated significantly in the last quarter, when GFZ finally changed their thus far steadfast position, and announced that the spacecraft hardware was not in a state where it could support payload delivery at the scheduled delivery times. A minimum delay of two months was acknowledged. Responsibility for procurement and assembly of the sensor assembly portion of the instrument remained with AFRL, as it was for DIDM-1. The exception in this regard was provision of the wedge & strip anodes, for which Amptek retained its previous responsibility for design and manufacture. Details on the wedge & strip anode functionality and development effort, which proved to be a much more difficult proposition than was first envisaged, is presented in section 2.4. An immediate concern for both parties at the start of the characterization tests, was how well the measures taken by AFRL to refine the sensor design and improve measurement accuracy, worked. The intent was to reduce the size of the electron cloud which exited the micro-channel plate detectors, in response to an incident ion, and falls onto the positional sensitive *wedge & strip* anode, so that better positional resolution might be achieved. The definitive assessment is yet to be made, but preliminary indications show that these sensor improvements were successful. The drift meter image is much more tightly defined than has been previously observed. An illustrative example of this appears in Figure 2. It shows a map of the pixels being stimulated on the anodes of both sensors, while the instrument is in an ion beam, in the test chamber. Note that the active area is confined to a relatively small sector of the entire map, which is very desirable. The nominal display is in color, so that pixel counts can be easily discerned through the use of the associated color legend.
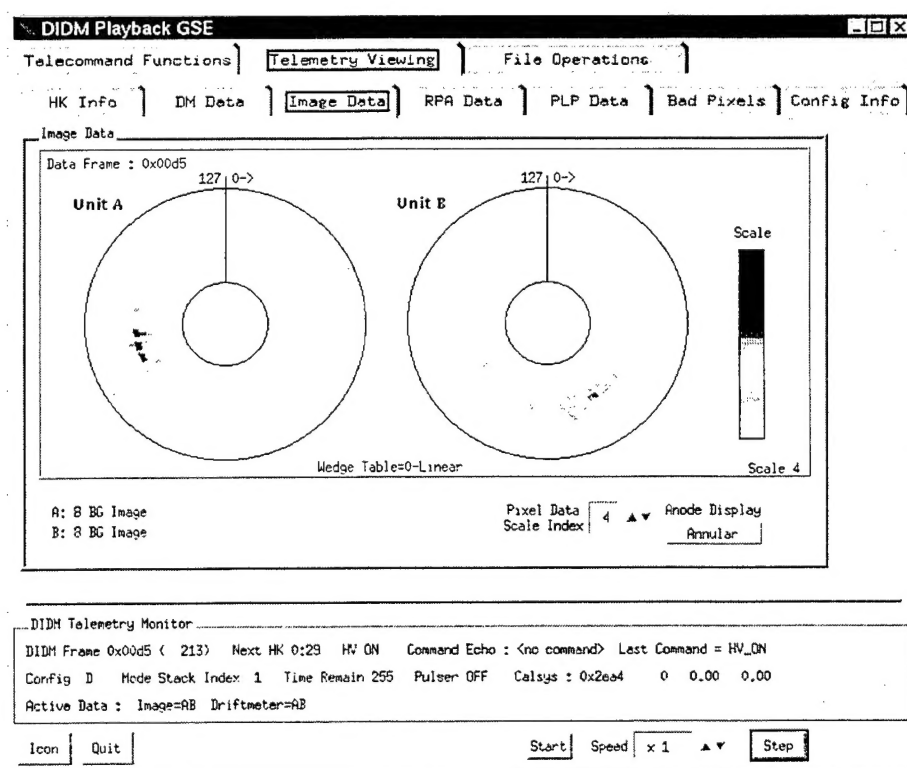

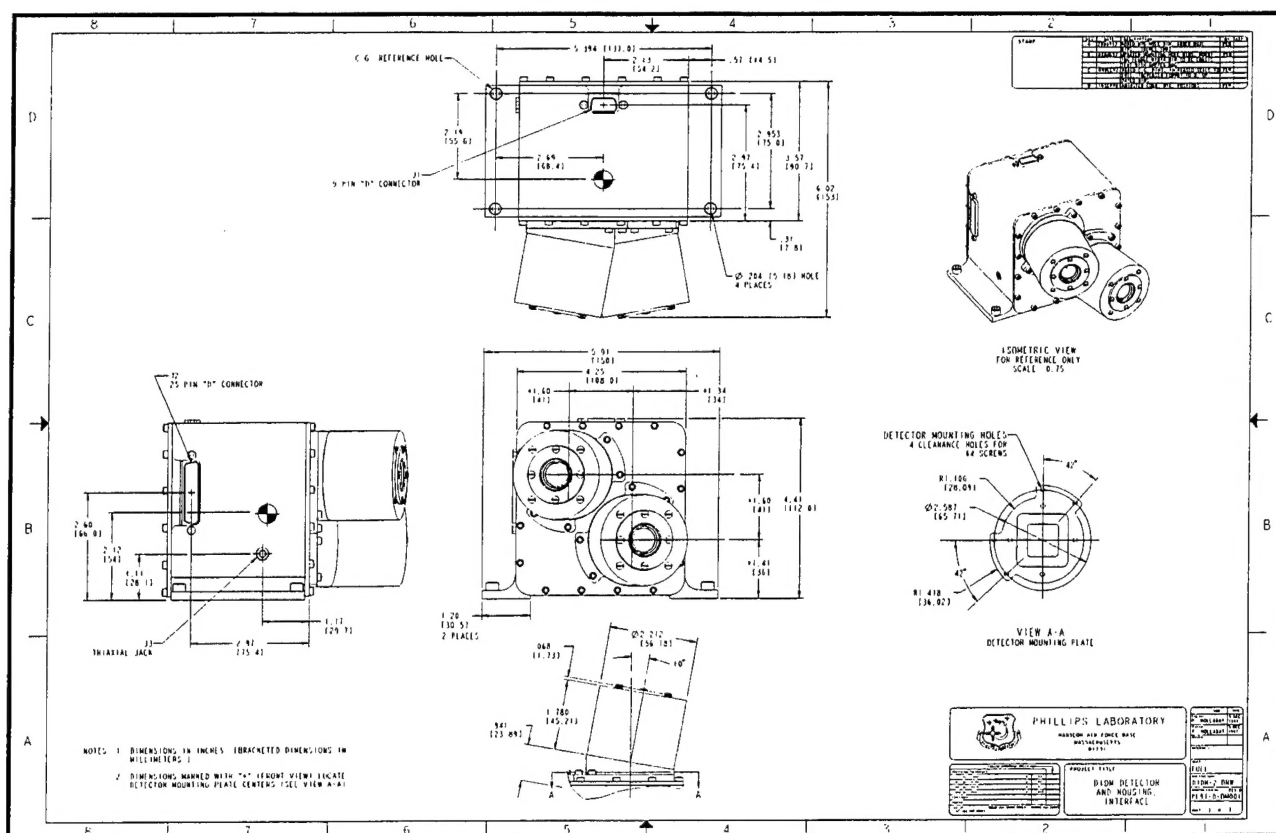FIGURE 2: GSE DISPLAY OF DIDM-2 DRIFT METER IMAGE DATA
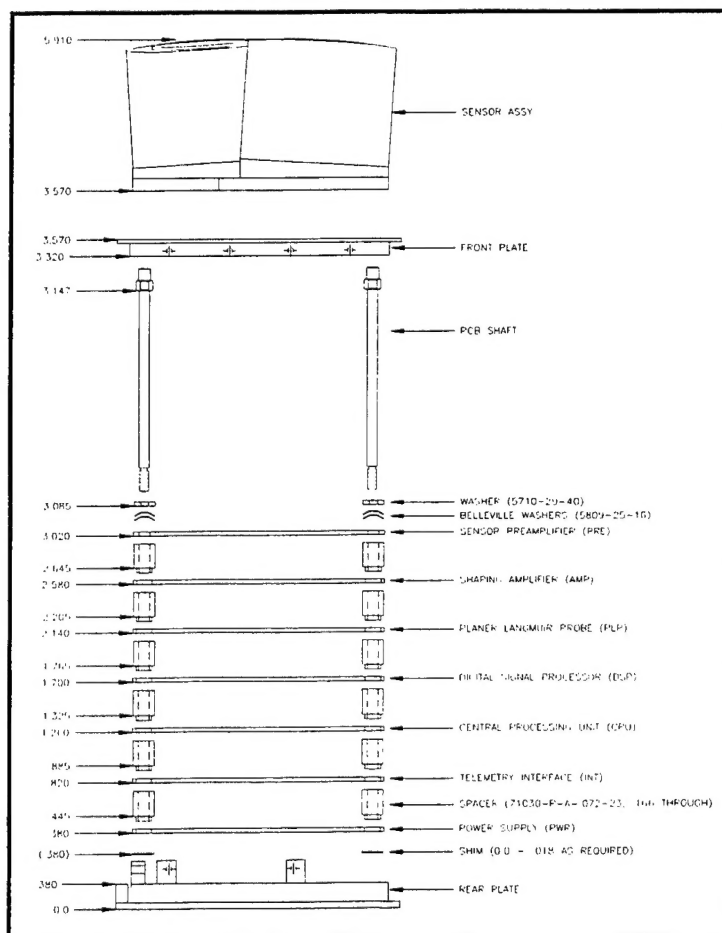
FIGURE 3: THE DIDM-2 INSTRUMENT

FIGURE 4: DIDM-2 BOARD STACK

2.3 DIDM-2 Hardware

The new DIDM instrument (shown in Figures 3 and 4) inherited much from its predecessor DIDM-1. Indeed the original proposal was to provide a duplicate of DIDM-1, incorporating only the changes necessary to make the instrument suitable for flight on the CHAMP spacecraft. Accordingly, the two instruments are virtually identical in appearance. However, significant changes have beeen made to DIDM-2, in part, to incorporate lessons learned from DIDM-1 and to satisfy environment requirements for the CHAMP mission. DIDM-2 was also made slightly longer to accommodate the electronics for the Planar Langmuir Probe (PLP), which was not a feature of DIDM-1.

The mounting arrangement of the instrument was changed from the separate, detachable, mounting rails used in the previous design, to one in which the mounting rails are now integral to the instrument housing. The DIDM-1 design was shown to have some inadequacies in its thermal transfer capability, which complicated the temperature control job for the instrument after integration on a spacecraft. Additionally, the electronics enclosure has also been thickened, from the 0.062" drawn shell used previously, to 0.190". This was done to provide as much shielding as possible, for the electronic components within the box. From design guidelines provided by the

FIGURE 5: CHAMP DOSE DEPTH CURVES

CHAMP program office, the thickened walls will ensure that the total dose received from high energy particles, inside the enclosure, be less that 1k Rads per year, in silicon. This is significant shielding since the program requirement is for survivability with a maximum of 5k Rads per year. The inherent radiation hard capabilitity of most of the electronic components ensures that the requirement is satisfied, but a few components are used which were not specifically designed to be rad-hard, and for these the shielding provided by the enclosure will be significant (although not critical) to their survival. The Dose Depth Curve for the CHAMP mission is shown in Figure 5.
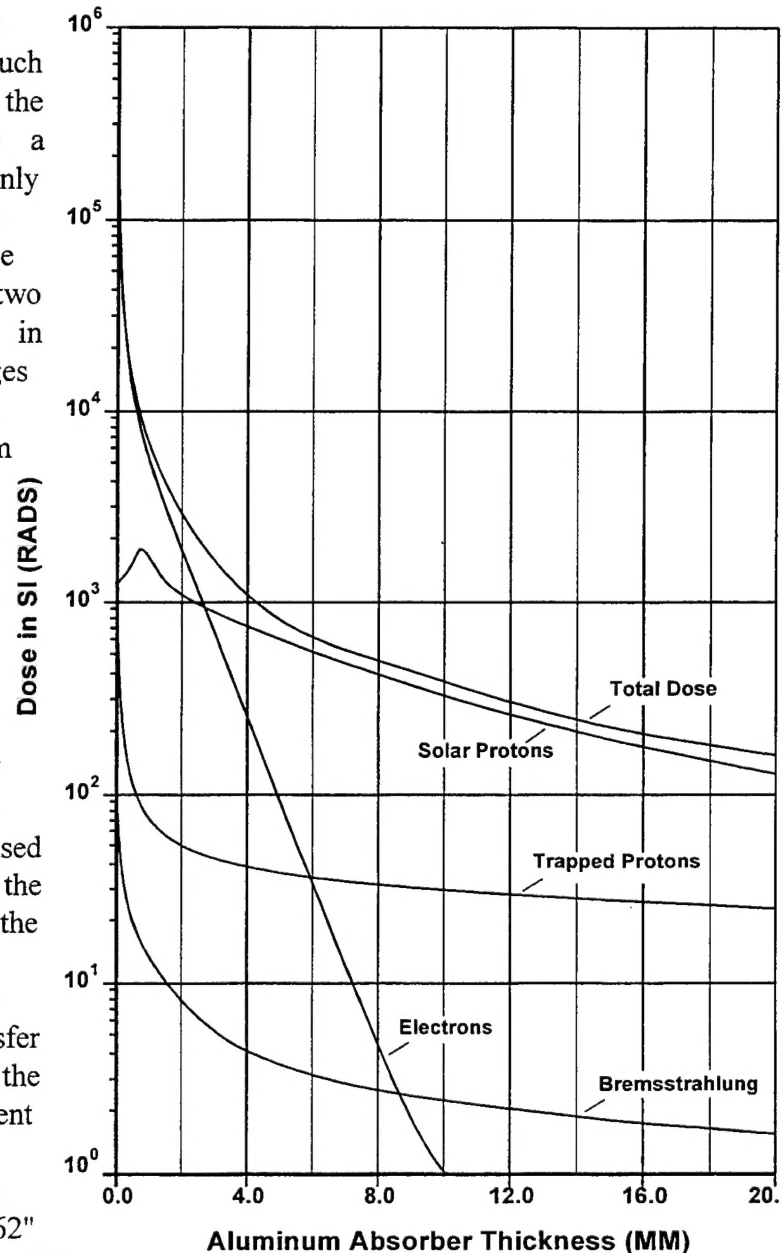
2.4 Wedge & Strip Anode

Incident ions are detected within the sensor elements at the front of the DIDM instrument. The particles are first focused onto a MicroChannel Plate (MCP) detector, which generates an electron cloud, that strikes a uniquely designed *wedge & strip* anode, at a position corresponding to the incident angle of the ion at the sensor aperture. The location on the anode is provided by the respective amplitude of signals from the wedge (W), strip (S) and z (area between wedge and strip) elements on the anode. There are 120 distinct segments on the DIDM-2 anode, with W, S, and Z elements within each. Polar angle (θ) is determined from the wedge elements, which are of constant size throughout, but vary linearly in area from the inner to outer regions of the anode. Minimum θ comes from a smaller wedge area than does maximum θ. In an equivalent fashion, azimuth angle (ϕ) is determined from strip elements, which are of a different size in each segment. The largest strip produces maximum ϕ, while the smallest produces minimum ϕ. The general relationships between wedge & strip elements and incident angles are:

$$\theta = \frac{K_\theta \times W}{W + S + Z};$$

$$\phi = \frac{K_\phi \times S}{W + S + Z}$$
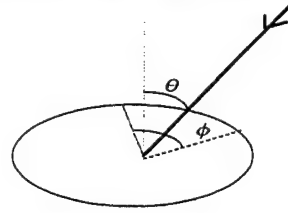
where K_θ and K_ϕ are the associated constants which ensure that the determined angle falls within the acceptance cone for the aperture (designed to be $\pm 45°$, but limited to $\pm 35°$ in DIDM-2 sensors). For the wedge & strip design to work properly, it is necessary that the diameter of the impinging electron cloud be approximately two elements wide. Smaller spot sizes could result in incorrect reporting of location, while much larger spots will not be as accurate. The anode design is optimized for a spot size of $\approx 0.060"$. A dimensioned schematic of the anode and an enhanced view of a small portion of the surface, clearly showing the anode elements and a typical electron spot, is shown in Figure 6.
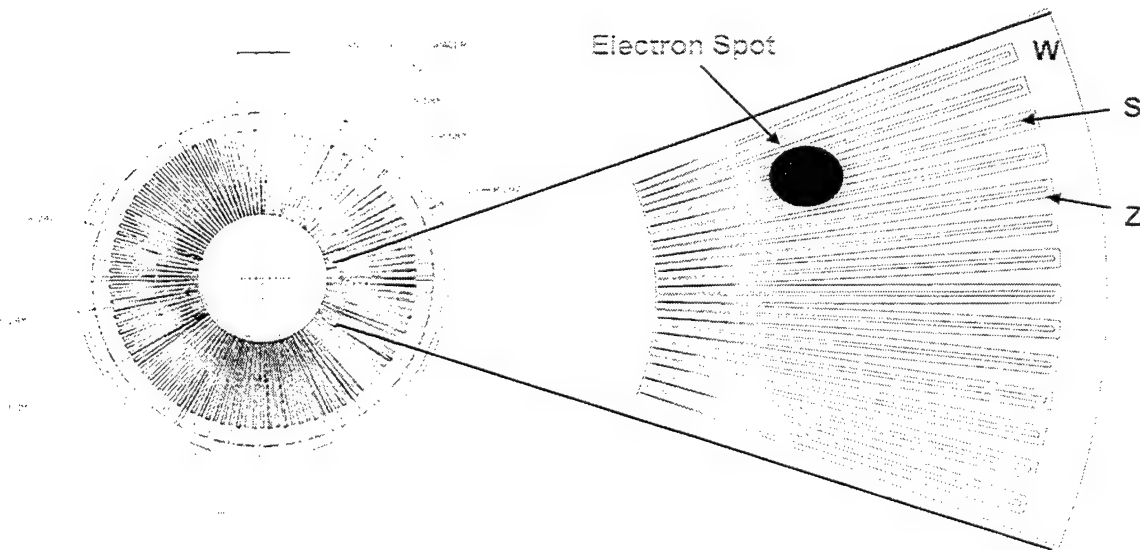

FIGURE 6:
WEDGE & STRIP ANODE PATTERN ELEMENTS
AND TYPICAL ELECTRON SPOT SIZE

To more easily identify the impact location on the anode surface, the active area (i.e. that portion within which valid events could occur) is mapped into 16 x 128 pixels. Polar angle (θ) is mapped into 16 radial elements *(r)* and azimuth angle (ϕ) is mapped into 128 circumferential elements *(c)*. It is therefore possible to identify an incident particle location to within any one out of a total of 2048 pixels. Each pixel is uniquely identified by combining its ring and column addresses. Example: r1c1, r5c99, r16c128 etc.

2.4.1 Active Area

The active area is that portion of the anode surface within which electrons are expected to fall. It is the physical extent encompassed by the rows in the pixel map, and is shown as the unshaded region in the schematic shown in Figure 7. The innermost limit is determined by an annulus on the MCPs. This limits the inner extent of the active area to 0.302" radius. The outer extent is set by the back-plane wall of the sensor. This is at 0.5018" radius.

FIGURE 7: SCHEMATIC SHOWING EXTENT OF ANODE'S ACTIVE AREA
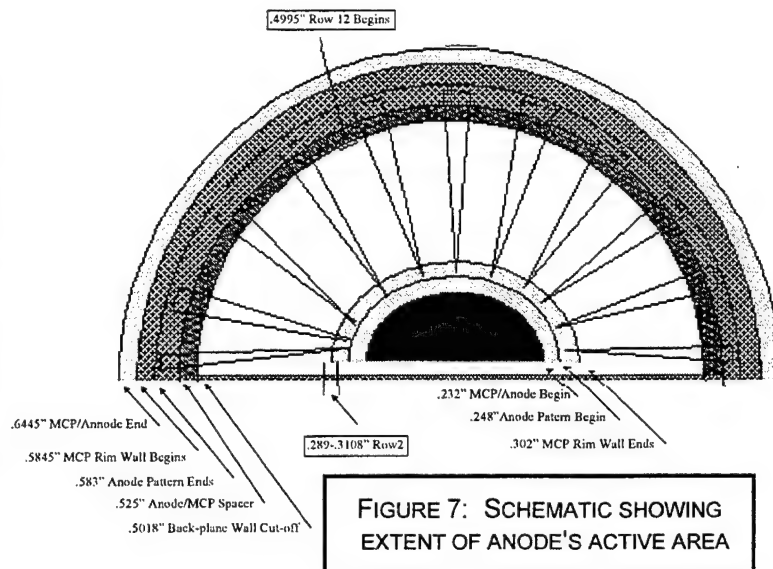
2.4.2 Zero-Crossing Mask

It is necessary to clearly demarcate the boundary between azimuth angles 0° and 360°. i.e. between c1 and c128 on the pixel array. Due to the physical size of the anode elements, which by design are much smaller, the output electron cloud will overlap this boundary, and if an incident trajectory were to produce a response in the area, a false azimuth position halfway between the two ends will be reported. It is therefore important that this outcome be precluded. The ideal way to do so would be to use MCPs that are not responsive in the area in question, and while this is no doubt possible to achieve practically, the cost of such a custom MCP fabrication effort is prohibitive. The next best thing therefore, is to put a physical barrier in position above the anode surface, which prevents the electron cloud from getting to the boundary crossing area. In DIDM, the zero-crossing mask is actually placed between the two halves of the chevron type MCPs. It turns out that this is the best place for such a barrier for reasons of mechanical support, and to prevent the possibility of differential charge build-up, which might preferentially steer the exiting electron cloud and/or give rise to capacitive coupling effects at the anode.
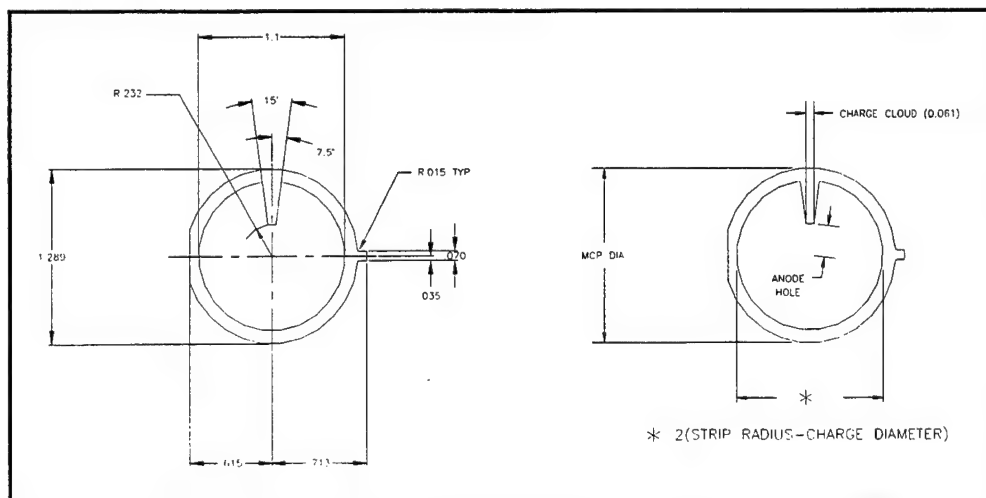

FIGURE 8: ZERO CROSSING MASK

The Zero Crossing Mask is made from thin (0.001"), electro-polished stainless steel and is designed such that an electron spot size diameter of 0.060" will not bridge the minimum and maximum azimuth elements. A dimensioned schematic is shown in Figure 8.

2.5 Anode Fabrication

Making DIDM anodes is a challenging task for the following reasons: (i) feature sizes within the DIDM anode pattern and (ii) the size of the anode. The width of the line which separates the wedge (w), strip (s) & intermediate (z) areas of the pattern is $5\,\mu m$ wide. The minimum width of these areas is also $\approx 5\,\mu m$. With feature sizes of this magnitude, photo-lithographic techniques must be used to reliably and cheaply generate multiple copies of the pattern. On the other hand, the anode occupies an area of almost one square inch and this is inordinately large to be patterened by this means. As an illustration, integrated circuits (ICs) are routinely made by photo-lithographic techniques, by mass production means these days. However, the typical size of an IC is less than a tenth the size of the DIDM anode and the difficulty of achieving a satisfactory yield using photo-lithographic fabrication techniques, increases almost exponentially with pattern size.

2.5.1 Photo-lithographic process

The photo-lithographic process is a very exacting one, in that particulate contamination has to be controlled to the utmost extent. With these feature sizes, dust, lint or hair particulates could easily give rise to pattern defects, which would be manifested, in undesirable shorts or open circuits somewhere on the pattern. In the integrated circuit (IC) fabrication business where the techniques were developed, it is usual to anticipate a certain loss percentage due to defects. Given that the typical IC area is one tenth the size of the DIDM anode, the nature of this concern is clearly different here. Making DIDM anodes is more exacting in this regard since not only is the pattern very much larger than usual, but since only a handful are being made, in principle only zero defects can be tolerated.

The steps involved are as follows: (i) a master copy of the pattern is made by *writing* (either by laser or e-beam) into a soda lime substrate, which is coated first with Chromium (Cr) and then with photo-resist. The actual writing is done into the photo-resist material, and the pattern is actually etched into the Cr. Typically, these masks are 0.090" thick and the Cr is $\approx 1000\,\text{Å}$ thick.

(ii) contact prints of the master are then made. To do this, a blank quartz substrate is metalized (wafer and substrate are synonymous terms. They refer to the quartz [SiO_2] material from which the anodes are made. 4" x 4" square and 3½" dia. round ones are the two sizes that have been used for DIDM. Vendors prefer one or the other geometry) and photo-resist coated. The master is then laid on top of the photo-resist-coated/metalized substrate and back illuminated with UV. The pattern is transferred into the photo-resist by this means, and then etched into the substrate.

The only photo-resist-coated/metalized substrate which can be bought off-the-shelf are the Cr substrates for making masks. All others must be custom made. This fact introduces several difficulties. The most significant of these are: (i) finding suitable vendors to do the work. (ii) finding ones willing to provide the small quantity required, at an affordable price. The issues involved here will be addressed in turn.

Mask making houses routinely make IC patterns of even tighter feature sizes (state-of-the-art is now approaching $0.1\,\mu m$), albeit on much smaller than anode sizes, and in quantities of hundreds of thousands. They start with procured photo-resist coated Cr substrates, which are defect free. i.e. there is virtually no particulate matter in the photo-resist material or in the Cr coating. The manufacturing environment in which these processes are carried out is such that process defects are eliminated. For example, photo-resist is usually applied in a class 1 environment (which means one

particulate per cubic centimeter or less). Also, since only Cr is etched and the thickness is unvarying, the etching techniques to reliably achieve the minimum feature size has become well known and the process is very much a science rather than the art-like craft it is otherwise.

2.5.2 Why custom-made

These advantages are all lost in the custom-made realm of the DIDM anodes. To begin with, it is necessary to find a vendor who is willing to undertake the entire project. i.e. metalization, photo-resist coat, patterning and etch. Also, in order to minimize cost, the vendor should execute all of these steps himself. There are only a handful of companies throughout the country who advertise this capability, for the quantities of interest to the program. Such a vendor is unlikely to have a class 1 facility in which to do the work. The usual quoted capability is class 10,000. Inevitably then, the possibility of process defects will be significantly increased. In addition, because the metalization required is not simply Cr, finding the right combination of etch concentration, time and temperature is very much an art rather than a science, and this adds considerably to the yield equation. It can be expected that fewer good parts will be realized than would be the case if regular production methods were utilized.

2.5.3 Process complexity

For reasons which will be explored in a later section, it is required that the anodes be Gold (Au) coated. Au will not easily adhere to quartz, so it is necessary to have a binding layer of another material underneath the Au. This could be Cr, but Nichrome (NiCr), Titanium/Tungsten (Ti/W) and Copper (Cu) are also suitable alternatives. All have been tried. The choice of the binding layer is a vendor's choice and is dependant on his metalization capability and etch expertise .

The metalization process is carried-out in a vacuum chamber. The techniques used are vacuum sputtering or evaporation of the metals from a heated bath to the target substrate. By sequentially heating the metals, each can in-turn, be made to coat the substrates without any adhesion problems. One vendor used a binding layer of 300 Å of Cr, underneath 2000 Å Au. 300 Å Ti/W was used to coat the Au, on top of which the photo-resist was placed. The pattern was imaged into the photo-resist. The Ti/W was removed in the final wet etch step. In addition to the usual two photo-resist etch steps then, three metal etch steps were executed to remove Ti/W, Au and Cr. It must be emphasized that there is no formulaic solution to carrying out these metal etch steps. It is very much a trial and error (acquired through experience) process to get to the point where the pattern is properly completed with the required feature sizes. Over etching to achieve an unacceptable pattern occurs better than 50% of the time, and equally unacceptable patterns frequently result from under etching.

One reason why other metals are used as the binding layer material, is that compared to Cr, they are easier to etch. Ti/W for example, is supposed to be more forgiving than Cr and hence is not as easy to over-etch. The etchant for NiCr is supposedly not as concentration critical and hence is easier to use, in that regard.

2.5.4 Alternate approach

The DIDM anode was initially conceived with Cr coated quartz substrates in mind. The ease with which IC masks are made was known, and it was thought that replicating the process for the anode pattern would be trivial. It has not turned out that way. The quartz anodes are too resistive for use in this application. The net impact is that the z signal becomes non-linearly distorted over the path length to the anode contacts, and the signal electronics consequently generate a false report for the location of incident ions.

This is not a matter which could be compensated for or calibrated out. The only solution lies in lowering the resistivity of the surface material. To this end, various thickness of Cr were investigated. In the range from nominal thickness (1000 Å) to maximum available (8000 Å) the resistivity of Cr varies from 40 ohms/square to 2 ohms/square. The measured value for ≈ 2000 Å of Au was 0.4 ohms/square, which says that Au is still at least two orders of magnitude better. Electroplating the easy-to-obtain Cr anodes with Au has also been tried. Several commercial electroplating houses were approached to attempt either electrolytic or electroless plating. After several weeks and many attempts, all reported that their initial fears were confirmed. i.e. Cr is too passive a metal to be electroplated with Au.

3. TASK #2—DATA ANALYSIS EFFORTS

3.1 Program Definition

The objective of this task is to analyze the interactions between rockets and spacecraft with the space environment, in order to advance the understanding of dynamic space plasma effects. Efforts have been directed toward the analysis of data from the Tethered Satellite Systems flights (TSS-1 and TSS-1R), and the Space Wave Interactions with Space Plasmas Experiment (SWIPE) flown on the Observation of Electric-field Distributions in Ionospheric Plasma: a Unique Solution (OEDIPUS-C) mission and most recently, the data from the LAngmuir TURbulence (LATUR) rocket mission.

The work is concerned with characterizing electron beam-space plasma interactions and the dynamic I-V particulars of a magnetized plasma. Such knowledge of the space plasma environment and of its interactions with spacecraft is critical to the design of future platforms in space. It is expected that the work will advance the state-of-the-art capability of Air Force assets in the low earth orbit environment.

3.2 Summary of Activities

Work continued on the analysis of the OEDIPUS-C and SPREE datasets throughout the report period. In the latter half of the year, following the successful launch of the Langmuir Turbulence rocket mission from the NASA launch range in Puerto Rico, LaTUR data were added to the effort. Customized analysis software was written under this task, in order to look at the returned data. Since the content and format of the datasets differ in fundamental ways, it was impossible to use previously written code for the job. Taking advantage of lessons learned from previous efforts in this regard, the new software accommodated the science user's need for flexibility in choosing various data parameters for analysis and display, to thereby optimize the science exploitation effort. Accordingly, one enhancement that was added to the LaTUR data analysis capability is the means for the user to easily design individual displays to suit different scientific aspects and aims.

The multi-window display system runs on a PC/Windows platform. It provides easy mouse clicking access to the data, and slices of 3-D energy color spectra are easily accessed as 2-D energy spectrum cuts or a lists of electron counts. Hardcopy printing of screen displays to attached printers is also an incorporated feature. Additional details on display features appears in section 3.3.
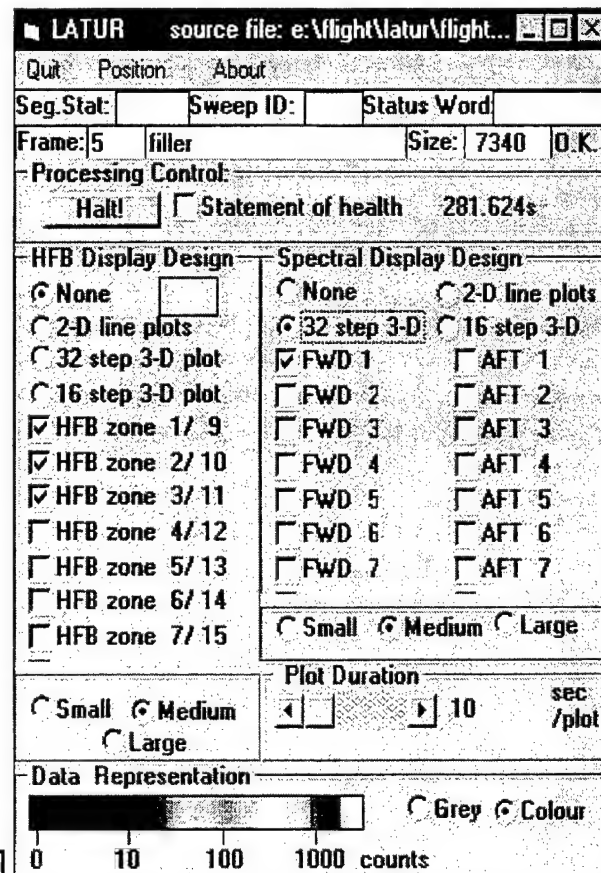
FIGURE 9: LaTUR ANALYSIS SOFTWARE DEFAULT DISPLAY

The OEDIPUS-C display software was also upgraded during the report period. The latest version now provides better synchronization to the data and some additional features. These include: ASCII file dumps of data for detailed numerical analysis, energy-frequency matrix with variable accumulation times, relative zone normalization by comparison of counts at low energy ranges, MAF identification, and a first attempt at automatic frequency analysis of the buncher data. The analysis capability of the software has also been improved, to the point where it is now capable of calculating and showing electron fluxes and distribution functions. Much of the improvement was prompted by the feedback received from participants at two scientific gatherings which the principal investigator for this work —Dr. Paul Gough, attended during the report period.

Two papers were presented at the Spring AGU meeting in Boston. The first entitled *MegaHertz Electron Modulations observed on TSS-1R*, dealt with SPREE data, whilst the other, *Sounder Accelerated Electrons observed on OEDIPUS-C*, presented new observations from the OEDIPUS-C mission. The encouraging response to the material gave added impetus to the work that was underway, in the period leading up to the first OEDIPUS-C experimenters meeting since the launch. Data from the OEDIPUS-C end of flight period was of particular interest, because that is where the plasma frequency increases above the electron gyrofrequency. This period is similar to TSS-1 and TSS-1R scenarios as well as to the situations prevailing in previous natural aurora rocket particle correlator measurements. The OEDIPUS-C experimenters meeting convened in Montreal towards the end of the report period, and by all accounts the material presented was well received.

Additional work is on-going to further analyze flight data for publication. Material is being prepared for an upcoming OEDIPUS paper to be published in the Journal of Geophysical Research, and a TSS-1R megaHertz electron modulations paper, which has been completed and was recently submitted to the Journal of Geophysical Research. The list of publications realized thus far from this effort is in section 3.5.

3.3 LaTUR Data Display Software

As previously mentioned, the LaTUR software has a startup form (see Figure 9) that permits easy customization of the data display. Any combination can be shown of the 8 Forward and 8 Aft electron zones for electron spectra, as well as, a selection from the 8 connected to the buncher electronics for the MHz displays. Also, the plot size has three possible values to best fit the data displayed on to the PC screen.

Figure 10 shows the instrument state of health monitor for the various housekeeping parameters. Two all-flight spectrograms are shown next in Figures 11 and 12, for the Forward and Aft electron zones respectively. The plots are nominally in color, but appear here in monochrome. Detailed short plot duration displays are also available for each of the seven zones shown.

🔳 Health	⊠◻⊠
Sub Frame lsb:	0EH
Sub Frame msb:	00H
Expt frame lsb:	D8H
Expt frame msb:	05H
Enc majfrm lsb:	AEH
Enc majfrm isb:	D2H
Enc majfrm msb:	00H
Enc minfrm lsb:	F0H
Enc minfrm isb:	4FH
Enc minfrm msb:	1AH
Output_PTR lsb:	00H
Output_PTR	3FH
Segment status:	4AH
Sweep ID :	07H
StatusWord lsb:	80H
StatusWord msb:	00H

FIGURE 10: LaTUR STATE-OF-HEALTH MONITOR DISPLAY
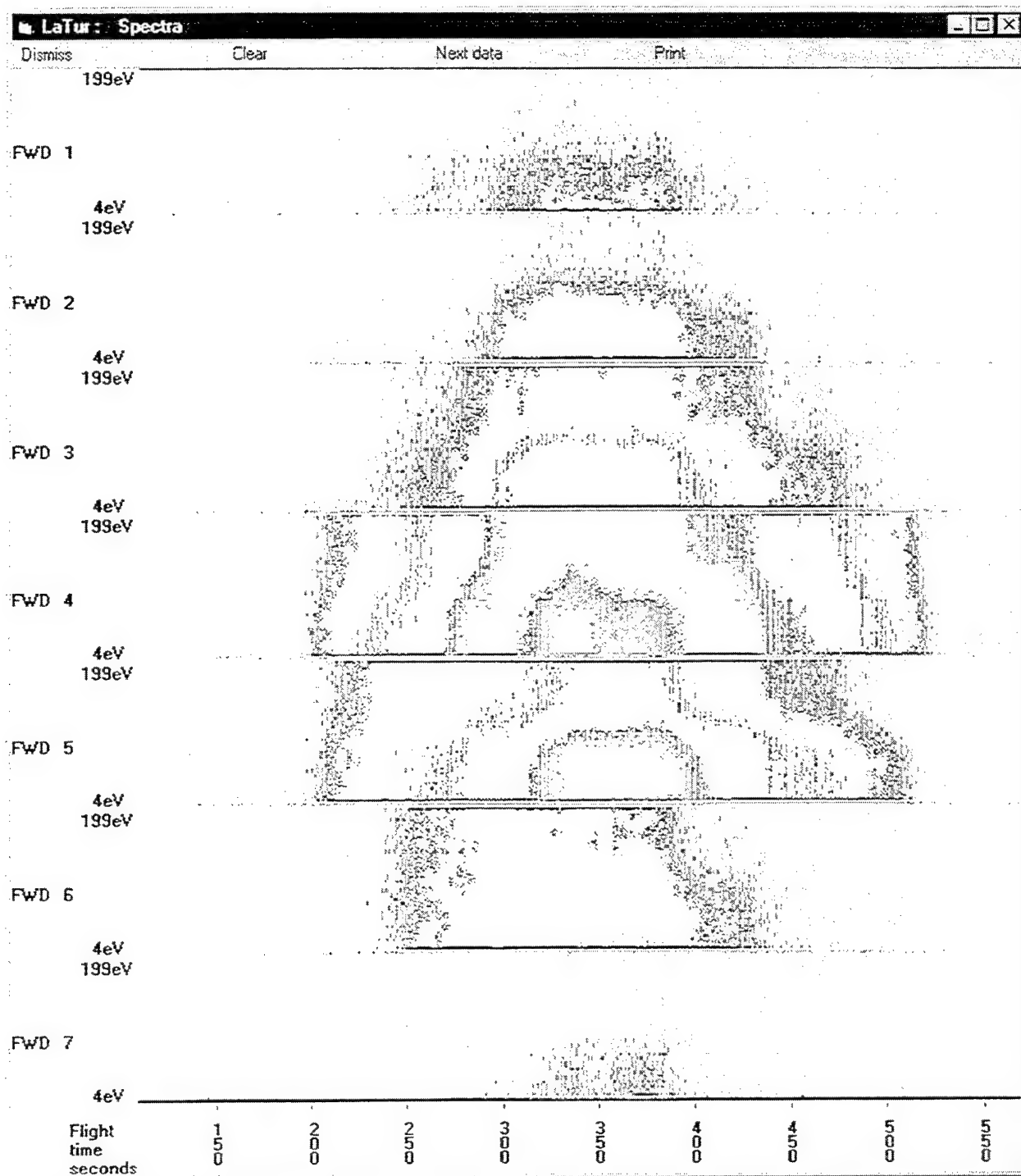
FIGURE 11: ALL FLIGHT SPECTRA FOR FORWARD SENSOR ELECTRON ZONES.
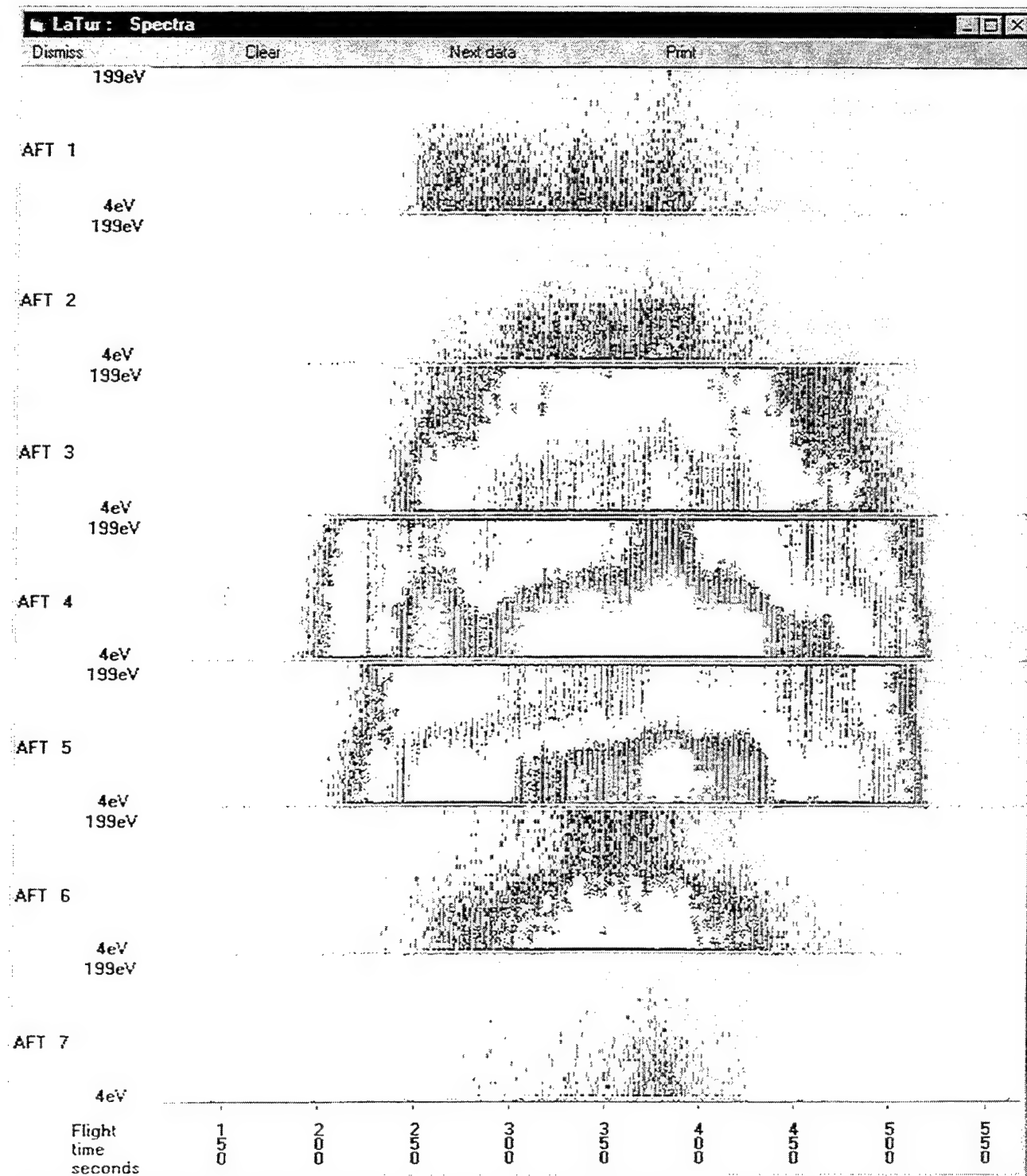
FIGURE 12: ALL FLIGHT SPECTRA FOR AFT
SENSOR ELECTRON ZONES.

Clicking the mouse once on either of Figures 11 or 12 above, results in the 2-D electron spectrum seen in Figure 13(a). Clicking once more yields the actual electron count spectrum listing (Figure 13(b)).
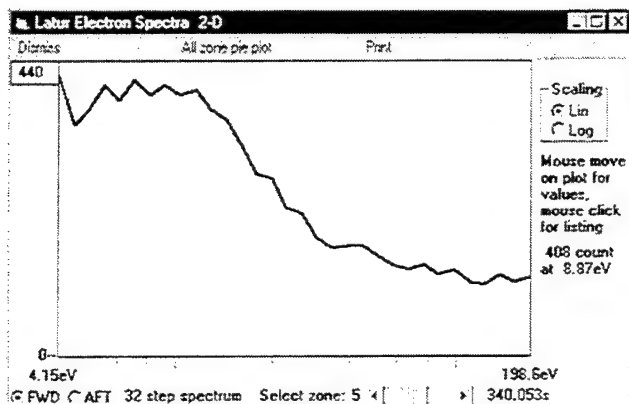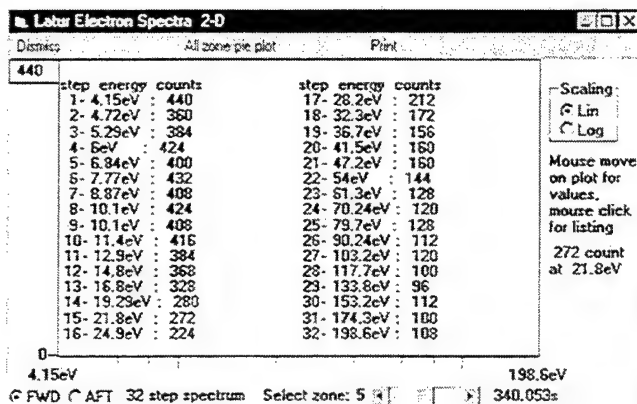
(a)   (b)

FIGURE:13: (a) 2-D SPECTRUM CUT;
(b) LISTING

3.4 OEDIPUS-C EPI.Display Software

FIGURE 14: ELECTRON ZONE PLOTS

The absolute geometric factors have now been included within the software so that both relative zone plots now match better (Figure 14). Absolute flux values are also now available (Figure 15 (a), (b)). Fine re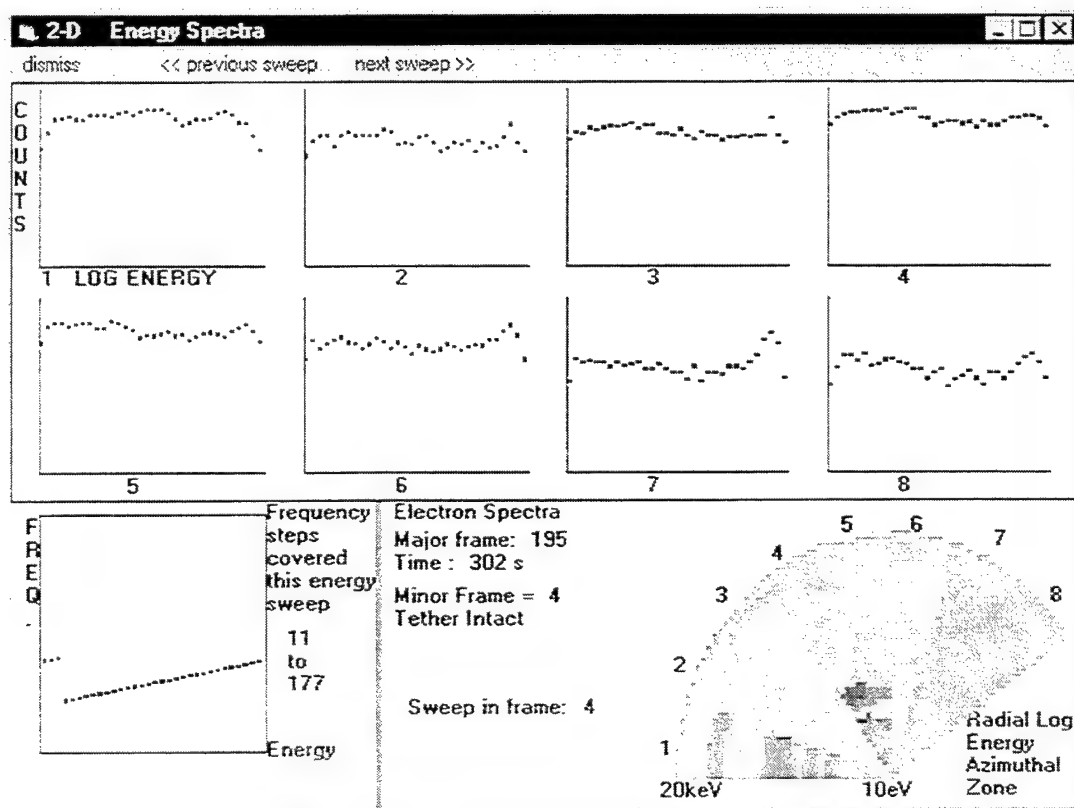solution MMU plots of electron response to the transmitter (Figure 16) pulse during an electron step have been modified to give a better plot for comparative response studies:
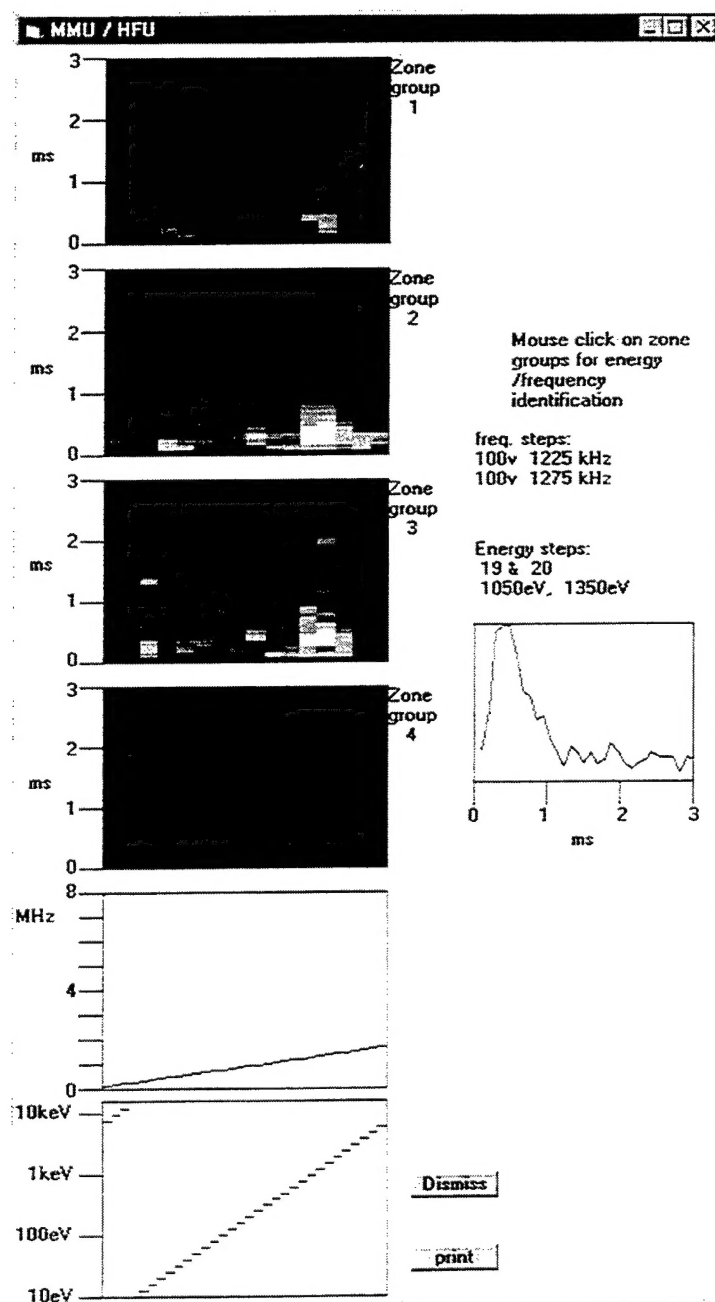

FIGURE 16: FINE RESOLUTION ELECTRON RESPONSE

Raw Count Data Values — Unit # 7 [1 of 8]

Energy	count	Diff.Flux	Distrib.Fn.F[E]	Fstep	Minor fr.	TX setup	Time order	HiRes Ebin
11	24	1.73e+03	2.55e-24	65	4	100v 3075 kHz	29	8
14	56	1.13e+03	1.30e-24	66	4	100v 3125 kHz	30	9
18	48	5.68e-07	5.11e-25	67	4	100v 3175 kHz	31	9
22	52	3.54e-07	2.61e-25	36	4	100v 1625 kHz	0	10
28	50	2.30e-07	1.33e-25	37	4	100v 1675 kHz	1	10
36	48	1.78e-07	8.01e-26	38	4	100v 1725 kHz	2	11
45	42	5.41e-06	1.95e-26	39	4	100v 1775 kHz	3	11
56	43	4.84e-06	1.40e-26	40	4	100v 1825 kHz	4	12
71	44	2.83e-06	6.59e-27	41	4	100v 1875 kHz	5	12
90	46	1.91e-06	3.45e-27	42	4	100v 1925 kHz	6	13
116	48	1.21e-06	1.69e-27	43	4	100v 1975 kHz	7	13
148	38	8.94e-05	7.60e-28	44	4	100v 2025 kHz	8	14
190	38	7.25e-05	6.19e-28	45	4	100v 2075 kHz	9	14
242	46	5.86e-05	3.93e-28	46	4	100v 2125 kHz	10	15
310	38	3.27e-05	1.71e-28	47	4	100v 2175 kHz	11	15
396	34	2.09e-05	8.56e-29	48	4	100v 2225 kHz	12	0
506	34	1.39e-05	4.45e-29	49	4	100v 2275 kHz	13	0
646	26	7.78e-04	1.95e-29	50	4	100v 2325 kHz	14	1
826	42	3.81e-04	1.92e-29	51	4	100v 2375 kHz	15	1
1050	25	4.63e-04	7.14e-30	52	4	100v 2425 kHz	16	2
1350	34	5.70e-04	6.84e-30	53	4	100v 2475 kHz	17	2
1720	34	4.14e-04	3.90e-30	54	4	100v 2525 kHz	18	3
2200	31	2.96e-04	2.18e-30	55	4	100v 2575 kHz	19	3
2812	42	4.07e-04	2.34e-30	56	4	100v 2625 kHz	20	4
3590	42	3.55e-04	1.60e-30	57	4	100v 2675 kHz	21	4
4590	38	2.83e-04	9.99e-31	58	4	100v 2725 kHz	22	5
5870	50	4.00e-04	1.10e-30	59	4	100v 2775 kHz	23	5
7500	64	5.65e-04	1.22e-30	60	4	100v 2825 kHz	24	6
9580	108	6.00e-04	1.01e-30	61	4	100v 2875 kHz	25	6
12200	140	4.73e-04	6.28e-31	62	4	100v 2925 kHz	26	7
15700	96	2.58e-04	2.86e-31	63	4	100v 2975 kHz	27	7
20000	28	8.80e-03	7.13e-32	64	4	100v 3025 kHz	28	8

(a)

Raw Count Data Values — All 8 zones Electron distribution Function $f(cm^2 * sr\, eV)$:

eV	1	2	3	4	5	6	7	8	TX setup
11	2.15e-24	2.26e-24	1.52e-24	5.62e-25	1.13e-24	1.80e-24	2.55e-24	5.64e-25	100v 3075 kHz
14	1.09e-24	9.13e-25	5.82e-25	3.65e-25	8.08e-25	9.08e-25	1.30e-24	2.96e-25	100v 3125 kHz
18	3.73e-25	2.71e-25	2.55e-25	1.34e-25	2.91e-25	2.58e-25	5.11e-25	1.45e-25	100v 3175 kHz
22	1.88e-25	1.71e-25	1.58e-25	7.68e-26	1.56e-25	1.76e-25	2.61e-25	5.35e-26	100v 1525 kHz
28	1.05e-25	5.43e-26	6.72e-26	4.26e-26	6.16e-26	7.84e-26	1.33e-25	2.53e-26	100v 1575 kHz
36	4.20e-26	3.72e-26	4.06e-26	2.46e-26	3.16e-26	5.49e-26	8.01e-26	2.13e-26	100v 1725 kHz
45	1.69e-26	2.13e-26	1.84e-26	1.36e-26	2.10e-26	1.84e-26	1.95e-26	7.03e-27	100v 1775 kHz
56	1.14e-26	1.03e-26	9.73e-27	8.21e-27	1.16e-26	9.83e-27	1.40e-26	5.21e-27	100v 1825 kHz
71	5.57e-27	4.45e-27	5.04e-27	4.28e-27	4.46e-27	4.39e-27	6.59e-27	3.45e-27	100v 1875 kHz
90	2.64e-27	2.28e-27	2.78e-27	1.91e-27	2.20e-27	2.70e-27	3.45e-27	2.22e-27	100v 1925 kHz
116	1.15e-27	1.24e-27	1.20e-27	1.13e-27	1.49e-27	1.73e-27	1.63e-27	1.15e-27	100v 1975 kHz
148	6.20e-28	6.96e-28	7.15e-28	6.43e-28	6.98e-28	8.04e-28	7.60e-28	6.65e-28	100v 2025 kHz
190	3.54e-28	3.20e-28	4.75e-28	4.17e-28	4.46e-28	4.13e-28	6.19e-28	2.79e-28	100v 2075 kHz
242	2.10e-28	1.93e-28	2.19e-28	2.15e-28	2.47e-28	3.21e-28	3.93e-28	1.40e-28	100v 2125 kHz
310	1.51e-28	1.14e-28	1.17e-28	1.21e-28	1.08e-28	1.75e-28	1.71e-28	5.91e-29	100v 2175 kHz
396	8.63e-29	5.35e-29	5.75e-29	5.58e-29	6.70e-29	8.51e-29	8.56e-29	4.08e-29	100v 2225 kHz
506	5.88e-29	5.20e-29	4.67e-29	4.00e-29	4.08e-29	6.96e-29	4.45e-29	2.85e-29	100v 2275 kHz
646	4.04e-29	3.47e-29	2.55e-29	2.77e-29	2.80e-29	3.74e-29	1.95e-29	1.05e-29	100v 2325 kHz
826	2.38e-29	1.70e-29	1.45e-29	1.69e-29	1.96e-29	2.03e-29	1.92e-29	8.35e-30	100v 2375 kHz
1050	1.36e-29	8.31e-30	1.21e-29	1.01e-29	1.08e-29	1.36e-29	7.14e-30	5.88e-30	100v 2425 kHz
1350	6.76e-30	5.68e-30	6.40e-30	6.45e-30	7.10e-30	8.73e-30	6.84e-30	4.44e-30	100v 2475 kHz
1720	4.54e-30	3.94e-30	3.91e-30	3.43e-30	3.64e-30	4.51e-30	3.90e-30	2.25e-30	100v 2525 kHz
2200	3.61e-30	2.66e-30	2.30e-30	2.83e-30	2.96e-30	2.85e-30	2.18e-30	1.41e-30	100v 2575 kHz
2812	2.64e-30	2.03e-30	1.77e-30	1.80e-30	2.39e-30	2.25e-30	2.34e-30	1.53e-30	100v 2625 kHz
3590	1.93e-30	1.04e-30	1.16e-30	1.29e-30	1.68e-30	1.63e-30	1.60e-30	1.01e-30	100v 2675 kHz
4590	1.52e-30	9.53e-31	8.56e-31	9.26e-31	1.07e-30	1.07e-30	9.99e-31	5.37e-31	100v 2725 kHz
5870	1.22e-30	6.15e-31	5.94e-31	7.07e-31	6.69e-31	9.73e-31	1.10e-30	4.69e-31	100v 2775 kHz
7500	7.81e-31	4.84e-31	5.15e-31	4.86e-31	5.85e-31	7.77e-31	1.22e-30	4.46e-31	100v 2825 kHz

(b)

FIGURE 15: (a) ABSOLUTE FLUX VALUES; & (b) ELECTRON DISTRIBUTION FUNCTION (obtained by clicking on pie in individual spectrum of Fig. 13)

3.5 Recent Scientific Publications from TSS-1/1R SPREE and OEDIPUS-C

3.5.1 Published:

Gough, M.P., Hardy, D.A., Burke, Oberhardt, M.R., Gentile, L.C., Huang, V.Y., Cooke, Raitt, W.J., Thompson, D.C. McNeil, W. and Bounar, K. Heating and low-frequency Modulation of electrons Observed during Electron Beam Operations on TSS-1; Journal of *Geophysics Research*, Vol 102, 1997, pp.17335-17357.

Gough, M.P., Burke, W.J., Hardy, D.A., Huang, C.Y., Gentile, L.C., Rubin, A.G., Oberhardt, M.R., Thompson, D.C. and Raitt, W.J. MegaHertz Electron Modulations Observed during TSS-1R Beam Emission Experiments; *Geophysics Research Letters*, Vol 25, 1998, pp.441-444.

Gough, M.P., Hardy, D.A., Oberhardt, M.R., Burke, W.J., Gentile, L.C., Thompson, D.C. and Raitt, W.J. SPREE Measurements of Wave-particle Interactions Generated by the Electron Guns on TSS-1 and TSS-1R; *Advances in Space Re*search, Vol.21, No.5, 1998, pp.729-733.

Gough, M.P., Hardy, D.A., and James, H.G. First Results from the Particle Correlators on the OEDIPUS-C Sounding Rocket; *Advances in Space Res.*, Vol 21, No 5, 1998, pp.705-708.

Gough, M.P. Particle Correlators in Space: performance, Limitations, Successes and the Future; pp 333-338. Measurement Techniques in Space Plasmas- Particles, AGU Monograph 102, 1998 ISBN 0-87590-085-2

Huang, C.Y., Burke, W.J., Hardy, D.A., **Gough, M.P.**, Olson, D.G., Gentile, L.C., Gilchrist, B.E., Bonifazi, C., Raitt, W.J., and Thompson, D.C. Cerenkov Emissions of Ion Acoustic like Waves Generated by Electron Beams emitted during TSS 1R; *Geophysics Research Letters*, Vol 25, 1998, pp.721-724.

3.5.2 Recently submitted to Journals:

Rubin A.G., Burke W.J., **Gough M.P.**, Huang, C.Y., Gentile L.C., Hardy, D.A., Thompson, D.C., Raitt, W.J. Megahertz Electron Modulations during TSS 1R; submitted to Journal of Geophysical Research, September 1998.

Huang C.Y., Burke W.J., Hardy, D.A., **Gough, M.P.**, James, H.G., Villalon, E., and Gentile, L.C. Electron acceleration by MHz waves during OEDIPUS-C; submitted to Journal of Geophysical Research. September 1998.

4. TASK #3—LaTUR EFFORTS

4.1 Program Definition

The objective of this task is to develop techniques to design and build miniaturized, low power and considerably more capable space experiment instrumentation. Current requirements necessitate reductions in size, mass, power consumption and telemetry bandwidth of diagnostic instruments on space platforms. A principal area of interest is in improving the performance of particle correlator hardware, while simultaneously reducing the size, mass and power requirements. Working with the Space Science Center (SSC) at the University of Sussex in the UK, Amptek, Inc. has been at the forefront of correlator development. The first correlator to be flown was provided by SSC in 1980. Since then, the collaborative effort has continually improved the capability of the units, by making use of the increased processing ability of new generations of hardware elements such as microprocessors and programmable gate arrays.

4.2 Summary of Activities

An improved correlator design was incorporated into the Data Processing Unit (DPU) that was provided by Amptek, Inc. for the Energetic Particle Instrument (EPI) suite, on the Langmuir TURbulence (LaTUR) rocket mission. The unit was completed after a period of intense activity, early in the report period. It was subsequently subjected to the required thermal and vibration tests, and then delivered by AFRL for integration onto the LaTUR rocket at the NASA Wallops Flight Facility around the middle of the report period. However, during the system vibration test of the LaTUR payloads, it was observed that the telemetry coming out of the DPU became anomalous during the thrust axis sine vibration test, at around 120 Hz. The state of the instrument's output was such that meaningless or "garbage" data was being returned, even though internal timing and event sequencing operations appeared to be nominal. When power to the unit was recycled after the test, normal operation was restored and the instrument properly survived subsequent random vibration testing in all three axis. It was determined after the sine vibration test, that due to structural resonance at the mounting location of the DPU, the instrument was being subjected to vibration levels in excess of three times the program limit, at the onset of the anomaly.

The DPU was returned to Amptek, Inc. where its anomalous output state was reproduced. It was demonstrated that in certain instances the instrument's "watchdog" timer (a software initiated instrument reset operation) was deficient. Under nominal conditions, the instrument checks for anomalous operational states every second and if any are detected operations are automatically re-initialized. This feature was clearly not working properly. The DPU operation software was rewritten to make the watchdog timer more effective. The particular deficiency which came to light at Wallops was eliminated and subsequent bench testing could not reproduce the condition. All of the nominal functional states of the instrument were also checked to ensure that the software changes did not have any unexpected impact on normal operation. The DPU was restored to flight configuration and retested to specified LaTUR payload test levels for sine and random vibration tests. The instrument performed nominally throughout the exercises.

The LaTUR rocket was launched on 11 Mar 98 at 23:11Z from the NASA launch range in Puerto Rico. The principal focus of this mission was to investigate wave-particle interactions as the rocket traversed a region of the ionosphere heated by a high power RF source from the Arecibo

Ionospheric Modification Facility. AFRL's EPI payload suite functioned nominally throughout the mission. EPI data were acquired and stored on the GSE (provided to AFRL by Amptek, Inc.) from both the forward and aft sensors. It was also observed that the returned HFB data properly switched from the forward to aft sensor after the payload switch command was sent to the DPU midway through rocket ascent. An overall picture of the returned data is shown in Figure 16. It is a nominal color plot, which shows the response (electron counts) from all eight zones of both the forward and aft ElectroStatic Analyzers (ESA). With the LaTUR mission now at an end, all work on this task is similarly concluded.
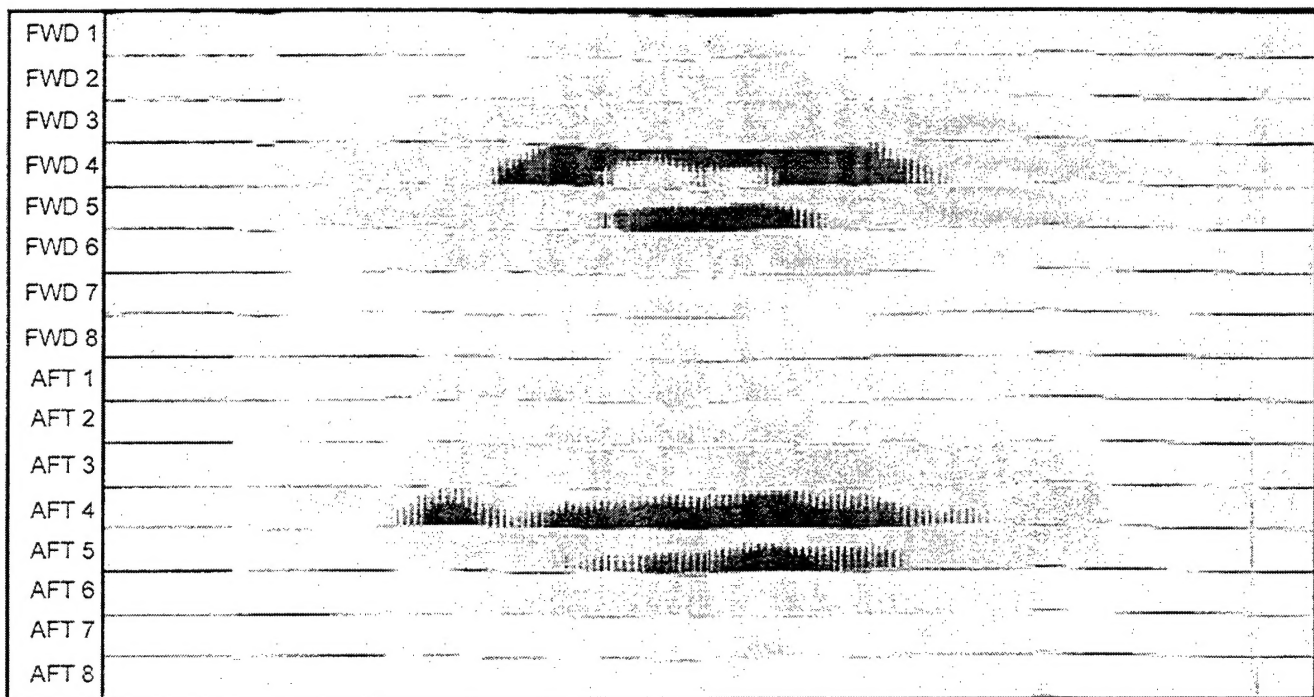

FIGURE 16: EPI ESA DATA FROM LATUR MISSION